Editors' Suggestion

Intrinsic hysteresis due to the surface barrier for chiral solitons in monoaxial chiral helimagnets

M. Shinozaki,[1] Y. Masaki,[2] R. Aoki,[3] Y. Togawa,[3] and Y. Kato[1,2]
[1]*Department of Basic Science, The University of Tokyo, Meguro-ku, Tokyo 153-8902, Japan*
[2]*Department of Physics, The University of Tokyo, Bunkyo-ku, Tokyo 113-0033, Japan*
[3]*Department of Physics and Electronics, Osaka Prefecture University, 1-1 Gakuencho, Sakai, Osaka 599-8531 Japan*

(Received 31 December 2017; revised manuscript received 8 May 2018; published 13 June 2018)

We present a theory of a surface barrier for isolated solitons to enter chiral magnets, in an analogous way to that of the Bean-Livingston barrier in the type II superconductors. With this theory, we discuss hysteresis observed in magnetoresistance (MR) measurements of monoaxial chiral helimagnet $CrNb_3S_6$. We argue that a large jump in the decreasing field process of MR of micrometer-sized samples is due to the disappearance of the surface barrier for the chiral soliton at a field $H = H_b$. This argument is justified through agreement between the experimental results at 10 K and our theoretical result $H_b/H_c = 4/\pi^2 \sim 0.4$ (with thermodynamic critical field H_c) based on the sine-Gordon model.

DOI: 10.1103/PhysRevB.97.214413

I. INTRODUCTION

Ordered states have generally their own rigidity [1] in their ground states; solids (crystals) exhibit elasticity, superfluids resist against rotating container and superconductors in the Meissner state refuse the entrance of magnetic field. Some of them also exhibit robustness even in metastable states; persistent currents in superfluids and superconductors in annulus geometry are examples. The metastability in those states owes to topological metastability in the sense that each flowing state is specified by a winding number of the phase of condensate wave function and this number takes a discrete value and thus cannot change continuously [2]. Those flows do not decay until phase singularities (solitons and vortices) are nucleated and phase slippage occurs [1]. Another example of topological metastability is irreversibility in magnetization curves in the type II superconductors, which is a manifestation of interplay between underlying topological defects (i.e., Abrikosov vortex [3]) and randomness (pinning centers) or surfaces of the specimen [4–6].

Chiral magnets also exhibit topological metastability. Metastability of skyrmions (magnetic vortices) [7–11] as an isolated object opens a possibility to a devise application. As an obvious consequence of the metastability, on the other hand, each skyrmion cannot be annihilated or created inside the samples without overcoming an energy barrier. Several ways to efficiently create [12–18] or inject [19,20] skyrmions inside chiral magnets have been proposed.

Cholesteric liquid crystals have physical properties similar to chiral magnets [21]; the field-induced cholesteric-nematic phase transition [22–24] is reminiscent of the continuous transition in chiral magnets [25–27] and it also shows metastability related to penetration of topological defect (π-kink) in the decreasing field process [23].

These examples illustrate the importance of topological metastability in various fields of condensed matter physics. In this paper, we present theoretically a prototype phenomenon of topological metastability near the boundary in chiral magnets and show that this phenomenon has been really observed in the experiments in a monoaxial chiral material $CrNb_3S_6$.

This paper is organized as follows: In Sec. II, we provide background of monoaxial chiral magnets: representative material $CrNb_3S_6$ (Sec. II A), its metastable property (Sec. II B), and the theory for equilibrium state (Sec. II C). In Sec. III, we present a theory of surface barrier for semi-infinite system (Sec. III A) and finite-sized system (Sec. III B). In Sec. IV, we compare our theory with experimental results of magnetoresistance (MR) measurements. In Sec. V, we discuss the importance of our findings in monoaxial chiral magnets in the context of similarity with the Bean-Livingston barrier in type II superconductors and other systems those exhibit continuous phase transition of nucleation type, which is one of the category of continuous phase transition that deGennes first classified [28].

II. MONOAXIAL CHIRAL HELIMAGNET

A. $CrNb_3S_6$

$CrNb_3S_6$ has a hexagonal layered structure consisting of NbS_2 layers with an intercalation of Cr atoms. The helical axis is the principal c axis and perpendicular to the NbS_2 layers. Each Cr atom has spin 3/2 and magnetic moment 3 μ_B [29,30]. Energy scales governing magnetic properties of this material are modeled as the intralayer ferromagnetic exchange interaction $J^\perp$, interlayer ferromagnetic exchange interaction J, interlayer Dzyaloshinskii-Moriya (DM) interaction D, and easy-plane anisotropy (with the c axis being the hard axis) K [29–31]. We ignore intralayer DM interactions, which are negligibly small (monoaxial approximation [31]). Among those scales, $J^\perp$ is dominant and we assume that the spin configuration is uniformly polarized in each layer, which is consistent with experimental observations [26]. Further, spins are considered as XY type owing to the presence of K and D. In the absence of magnetic field, competition between J and D results in a modulated spin structure in the form of simple helix with the propagation vector parallel to

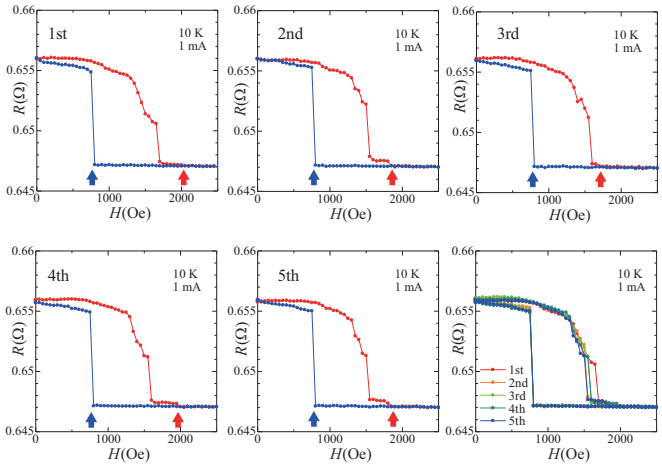

FIG. 1. Magnetoresistance in a micrometer-sized sample (sample A) of $CrNb_3S_6$ under in-plane magnetic field perpendicular to the helical axis. The specimen dimensions are 11.25 μm by 17.5 μm in the plane and 0.7 μm in thickness (17.5 μm width along the c axis). Each run (from first to fifth run) is given separately, while all runs are shown together in the lower-right panel. The blue and red arrows, respectively, indicate $H_{\rm jump}$ and $H_{\rm sat}$ for each run.

the c axis. Magnetic fields perpendicular to the helical axis distort the helical structure, which eventually transforms the uniformly polarized state [which is called forced ferromagnetic (FFM) state] at the thermodynamic critical field $H_{\rm c}$ of a continuous phase transition. The distorted helical structure (helicoid) in magnetic fields is recently called chiral soliton lattice (CSL) [31], in order to emphasize that it consists of underlying topological defects (single-discommensuration, 2π-kink, or domain wall [32], which we call chiral soliton.) The Lorentz transmission electron microscope and small-angle electron diffraction [26] showed that field-induced evolution of equilibrium states are well described by the Dzyaloshinskii theory for chiral magnets [25]. Thus $CrNb_3S_6$ can be regarded as a textbook example of chiral magnets. Our main interest in this paper is, however, metastability of this material [33–39].

B. Metastable property of $CrNb_3S_6$

In field-sweep processes, samples with different sizes exhibit hysteresis, which is often accompanied by discrete steps, in magnetization [29,30,34,35], MR [33,37,38], ferromagnetic resonance [36], magnetic torque measurements [38]. These observations imply the existence of underlying topological defect, i.e., chiral soliton and metastability responsible for hysteresis has a topological origin. Among those results, we focus on the MR measurements in micrometer-sized samples of $CrNb_3S_6$, which exhibit much larger hysteresis [33,37] than bulk [27,29,30,34,35]. The hysteresis of micrometer-sized samples in the MR consists of a conspicuous jump in the decreasing field process and a relatively gradual change in the increasing field process. Typical profiles have been presented in Fig. 2 of Ref. [33] and Fig. 1 in the present paper [40]. While the closing fields $H_{\rm sat}$ of hysteresis in the higher field side are near a thermodynamic critical field $H_{\rm c}$, earlier studies have not addressed a physical mechanism to govern the field $H_{\rm jump}$ where a discontinuous jump occurs in the MR in the decreasing field process. In the following part of this paper, we present a theory based on the sine-Gordon model and demonstrate that $H_{\rm jump}$ can be identified as a characteristic field $H_{\rm b} = 4/\pi^2 H_{\rm c} \sim 0.4 H_{\rm c}$ where the surface barrier disappears for chiral solitons to enter the samples. This theory agrees with experimental results on the MR of micrometer-sized samples of $CrNb_3S_6$ within a relative accuracy of several percent.

C. Summary of theory of monoaxial chiral magnets in equilibrium

As a prerequisite, we summarize the theory of field-induced state evolution of monoaxial chiral magnets in equilibrium. We start with the chiral-sine-Gordon model a la Dzyaloshinskii [25,41], which is reduced from the spin Hamiltonian or micromagnetic energy of chiral magnets. We take the helical axis (c axis) as the z axis and set the local spin at z as $\boldsymbol{S}(z) = S(\cos\varphi(z), \sin\varphi(z), 0)$ with the modulus S. Under the external magnetic field (strength H) parallel to the x axis, the energy of the chiral magnet occupying an interval I (which we specify in each case in the following discussion) in the z axis is given by

$$\mathcal{H}[\varphi] = JS^2 a_0 N_{2\rm d} \int_I {\rm d}z \left(\frac{1}{2}\left(\frac{\partial\varphi}{\partial z}\right)^2 - \frac{2\pi}{L(0)}\left(\frac{\partial\varphi}{\partial z}\right) - \left(\frac{m}{L(0)}\right)^2 \cos\varphi \right). \tag{1}$$

Here $N_{2\rm d}$ is the number of spins in each layer. $L(0)$ is $2\pi a_0 J/D$ with the interlayer distance a_0. The symbol m denotes the dimensionless coupling constant

$$m = (\pi^2/2)(H/H_{\rm c})^{\frac{1}{2}}, \quad H_{\rm c} \equiv \frac{\pi^2}{16}\frac{D^2 S}{J}. \tag{2}$$

The stationary condition yields the sine-Gordon equation

$$\frac{\partial^2\varphi}{\partial z^2} = \left(\frac{m}{L(0)}\right)^2 \sin\varphi \tag{3}$$

supplemented by the boundary condition

$$\left.\frac{\partial\varphi}{\partial z}\right|_{z\in\partial I} = \frac{2\pi}{L(0)}. \tag{4}$$

General solution to Eq. (3) is given by the Jacobi amplitude of the elliptic function [42],

$$\varphi(z) = \pi + 2{\rm am}\left(\frac{m}{\kappa L(0)}(z - z_{\rm s}), \kappa\right), \tag{5}$$

where κ denotes the modulus of the elliptic function. κ and $z_{\rm s}$ are constants of integral. We summarize the ground state property for infinite system derived by Dzyaloshinskii [25,41]. Substituting Eq. (5) into (1) for $I = (-\infty, \infty)$ and minimizing the energy with respect to κ, we obtain the ground state $\varphi(z) = 2\pi z/L(0)$+const. [simple helix with the period $L(0)$] for $H = 0$, $\varphi(z) = 0$ (FFM) for $H \geqslant H_{\rm c}$. For $H \in (0, H_{\rm c})$, the ground state is CSL described by Eq. (5) with κ determined by the relation ${\rm E}(\kappa)/\kappa = (H_{\rm c}/H)^{\frac{1}{2}}$ (${\rm E}(\kappa)$ is the complete elliptic integral of the second kind [42]). At $H = H_{\rm c}$, the energy of single soliton is zero in the infinite system.

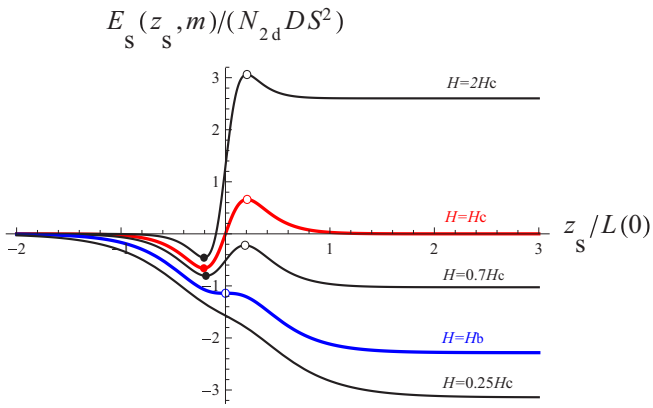

FIG. 2. Energy of the single soliton with respect to the uniformly polarized state (forced ferromagnetic state) as a function of the position of the soliton for several values of fields.

III. SURFACE BARRIER FOR SINGLE SOLITON IN MONOAXIAL CHIRAL MAGNET

A. Semi-infinite system

When we focus on the solution of a single soliton in chiral magnets occupying semi-infinite interval $I = [0,\infty)$, the modulus κ approaches unity from below and the function "am" reduces to the Gudemann function. For the moment, we ignore the boundary condition (4). The solution is then given by [43,44]

$$\varphi(z;z_s,m) = 4\arctan(e^{m(z-z_s)/L(0)}) \tag{6}$$

with the coordinate of the center of the soliton z_s, where Eq. (6) becomes π and $\boldsymbol{S}(z=z_s) = (-S,0,0)$. When $z_s = 0$ in Eq. (6), the soliton is located on the surface of the chiral magnet. The single soliton energy $E_s(z_s,m)$ is given by $\mathcal{H}[\varphi] - \mathcal{H}[\varphi = 0]$, the energy of the state with a single soliton subtracted by that of the FFM state. With use of Eq. (6), we obtain

$$\frac{E_s(z_s,m)}{4N_{2d}DS^2} = F(e^{mz_s/L(0)}), \quad F(X) = \frac{m}{\pi}\frac{X^2}{1+X^2} - \arctan X. \tag{7}$$

Figure 2 shows $E_s(z_s,m)$ as a function of z_s for several values of m. Equation (6) satisfies the boundary condition (4) when $\partial E_s/\partial z_s = 0$ and $|z_s| < \infty$. For $m \geqslant \pi \equiv m_b$, $\partial E_s/\partial z_s = 0$ for $z_s = \pm z_s(m)$ with

$$z_s(m) \equiv \frac{L(0)}{m}\ln\left(\frac{m}{\pi} + \sqrt{\left(\frac{m}{\pi}\right)^2 - 1}\right). \tag{8}$$

The points $(\pm z_s(m), E_s(\pm z_s(m)))$ in Fig. 2, respectively, correspond to the local maxima and minima, which are depicted by the open and solid circles.

We can see in Fig. 2 that the stable state for $H > H_c$ corresponds to the minimum at $z_s = -z_s(m)$ and thus is not uniformly polarized but the spin structure is distorted near the surface [the FFM state corresponds to the limit $z_s \to -\infty$ of Eq. (6)]. This state was discussed in Refs. [14,43–45], which has been called *surface twisted state* [44,45]. The distortion of spin structure near the surface in the cubic chiral magnets has been discussed in the study of skyrmions [14,19,20,46–51].

Compare this figure with Fig. 2 in Ref. [4] for *the Bean-Livingston barrier* for vortices in type II superconductors (H_c in the present case corresponds to the lower critical field H_{c1} in superconductors in Ref. [4]). Then one will see similarity between the single soliton energy in the monoaxial chiral magnets and single vortex energy when both are located near the surface. According to the theory in Refs. [4,5] for the Bean-Livingston barrier, the energy barrier for vortex to enter the type II superconductors vanishes at a threshold field, which is different from H_{c1}. Correspondingly, we see a threshold field in the present case is given by

$$H_b = (4/\pi^2)H_c \simeq 0.405285H_c, \tag{9}$$

below which the energy barrier for chiral soliton to enter the material vanishes.

In Fig. 2, the local minimum at a negative z_s survives down to $H = H_b$ and we see that the existence of the surface barrier at positive z_s and the local minimum at a negative z_s for $H > H_b$ is related with each other through the symmetry relation $E_s(z_s,m) - E_s(0,m) = -E_s(-z_s,m) + E_s(0,m)$. It follows that the surface barrier exists (does not exist) when surface twist exists (does not exist). The surface barrier and surface twist illuminate dual aspect of a single phenomenon.

Underlying energetics for formation of an energy barrier is easily understood; for simplicity we consider the case with $H = H_c$. In comparison with FFM state, a single soliton is favorable for DM energy but unfavorable for Zeeman energy and exchange energy. Thus the DM energy acts the attractive force (this energy term tries to invite the soliton to the inside) while the Zeeman energy and exchange energy act the soliton repulsion (these terms try to push out the soliton to the outside). The competition between the two generates the energy barrier. Note that the competing energies in surface barrier for vortices in type II superconductors are different from those in the present case; the screening current near the surface attracts vortices to the inside of the superconductors while the image vortex outside the sample attracts the vortices to the outside [4,5]. However, it is worthwhile to emphasize the similarity of surface barrier between the monoaxial chiral magnet and superconductors; the derivations of single soliton energy are analogous to that of single vortex energy (Ref. [5] is most appropriate to see this similarity). Further, both the surface barriers in the present case and the Bean-Linvingston barrier can be an intrinsic origin of hysteresis for the system that exhibits continuum phase transition in equilibrium case (we will remark again the similarity in the section Discussion).

Here we remark that Müller *et al.* theoretically addressed the penetration of chiral soliton into two-dimensional systems of cubic chiral magnets [20], where the solitons penetrate the material led by the penetration of merons in the field $H \leqslant 0.66H_{\rm kink}^{\rm cr}$ ($H_{\rm kink}^{\rm cr}$ denotes the magnetic field where the energy of single soliton becomes zero in cubic chiral magnets). This penetration is caused by instability of magnons bounded near the edge with nonzero momentum along the edge. We expect that edge instabilities in general uniaxial cases can interpolate the edge instability in the monoaxial case (the present study) and that found in the cubic case (Ref. [20]) as the two limiting cases.

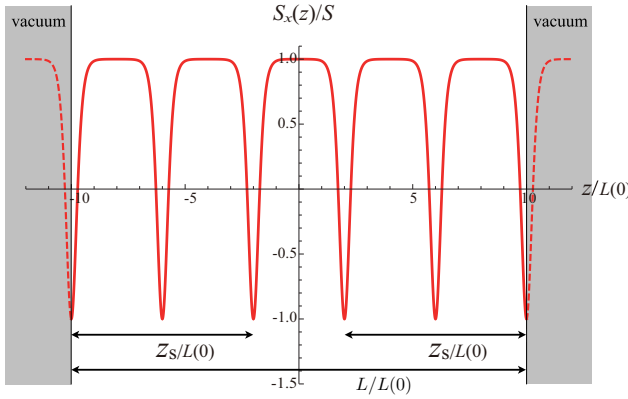

FIG. 3. Spatial distribution of the local magnetization at $H = H_b - 0$. We draw the $S_x(z)/S = \cos\varphi(z)$ inside the chiral magnet by the solid curve and its extension to the outside by the dashed curves. z_s is the distance between the position of the soliton closest to the center ($z = 0$) and the nearer boundary $z = \pm L/2$. Here we take $L = 20L(0)$.

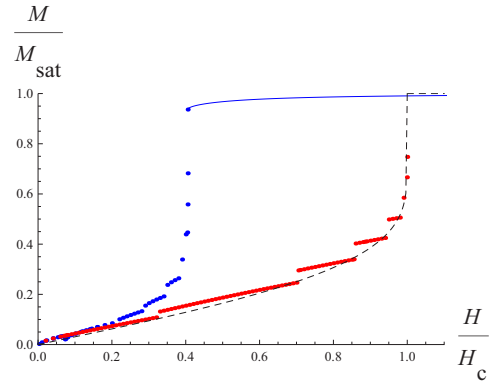

FIG. 4. M-H curve of metastable state in the decreasing field process for a finite size system with $L = 20L(0)$ is shown in blue dots. Blue curve represents approximate M-H curve Eq. (12) of the surface twisted states. M-H curve for energy minimum state for the finite size system (red dots) and that for infinite size system (dashed line) are also shown.

B. Finite-sized system

To see the effect of the surface barrier, we consider the evolution of the metastable states in decreasing field process in a finite-sized system. The chiral magnet occupies the interval $z \in [-L/2, L/2]$ of the length L along the helical axis. We consider the state with the closest soliton to $z = 0$ located at $z = \pm(L/2 - z_s)$. For the definition of z_s, refer to Fig. 3 [52]. The distance of the pair of solitons $L - 2z_s$ is equal to the fundamental period of the elliptic functions $2\kappa \mathrm{K}(\kappa)L(0)/m$. Here $\mathrm{K}(\kappa)$ is the complete elliptic integral of the first kind. With use of this condition, the state that we consider is given by

$$\begin{aligned}\varphi - \pi &= 2\mathrm{am}\left(\frac{m(z + z_s - L/2)}{\kappa L(0)}, \kappa\right) \\ &= 2\mathrm{am}\left(\frac{mz}{\kappa L(0)} - \mathrm{K}(\kappa), \kappa\right). \end{aligned} \tag{10}$$

Substituting Eq. (10) into Eq. (1), we obtain

$$\begin{aligned}\frac{E_s}{N_{2d} D S^2} = \frac{m^2 L}{\pi L(0)}\left(1 - \frac{1}{\kappa^2}\right) + \frac{4m\mathrm{E}(\kappa)}{\pi\kappa} - 2\pi \\ + \frac{4m}{\pi\kappa}\varepsilon\left(\frac{mz_s}{\kappa}, \kappa\right) - 4\mathrm{am}\left(\frac{mz_s}{\kappa}, \kappa\right), \end{aligned} \tag{11}$$

where $\varepsilon(u,\kappa)$ is the Jacobi's epsilon, which is defined as the integral of Jacobi's dn function $\varepsilon(u,\kappa) \equiv \int_0^u \mathrm{dn}(u',\kappa)\mathrm{d}u'$. We consider the evolution of metastable state in the decreasing field process starting with the surface twisted state above H_c (i.e., $m > \pi^2/2$). In this process, we specify the metastable state at m by $z_s(m)$, which is the smallest z_s among those satisfying $\partial E_s(z_s,m)/\partial z_s = 0$ and $\partial^2 E_s(z_s,m)/\partial z_s^2 > 0$. A more schematic description is given in the Appendix. Substituting Eq. (10) with $z_s(m)$ into the expression for the magnetization $\frac{M}{M_{sat}} = \frac{1}{L}\int_{-L/2}^{L/2} \cos\varphi \mathrm{d}z$, normalized by that of the FFM state M_{sat}, we obtain the magnetization curve of those metastable states in the decreasing field process, which is shown in Fig. 4 by blue dots for $H < H_b$. For $H > H_b$, we plot the approximate expression for the magnetization curve of surface twisted state

$$M/M_{sat} = 1 - (4L(0)/(mL))(1 - \sqrt{1 - \pi^2/m^2}), \tag{12}$$

which is equivalent to Eq. (24) of Ref. [44] and valid for sufficiently large system satisfying $e^{-mL/L(0)} \ll 1$. Further we also show the magnetization curves of the ground state for a finite-sized system with $L = 20L(0)$ (red dots) [53,54] and for the thermodynamic limit (the black dashed curve) in Fig. 4. In this figure, we can see a sharp drop in the magnetization curve of the metastable states (blue dots) around $H \sim 0.4H_c$ [55].

IV. COMPARISON WITH EXPERIMENTS

We now compare the theory with experimental results of MR for microsized samples of $CrNb_3S_6$ at a low temperature (10 K), which exhibit large hysteresis. Following Ref. [33], we consider that a large jump in MR results from discontinuous change in the soliton number. First we see experimental results for MR of thin samples with the c axis (the helical axis) in the plane under in-plane external magnetic fields perpendicular to the c axis and thus demagnetization effect is small. Figure 1 shows five runs of the MR data for the microsized $CrNb_3S_6$ specimens (sample A). We define H_{sat} as the magnetic field where hysteresis close in the higher field side of hysteresis loop and H_{jump} as the large jump occurs in MR in the decreasing field process. We see in Fig. 1 that the large jump in the decreasing field process is reproducible in the multiple runs in this measurement and we obtain $H_{jump} = 775$ Oe$\pm$25Oe, which we identify as H_b. We see that H_{sat} are scattered in the five runs as listed in Table I in the order of run of measurements from the first to fifth lines. The mean value of a set of the results $H_{sat}^{(i)}$ of the ith run is $\bar{H}_{sat} = 1895$ Oe and its uncertainty $\Delta H_{sat} \equiv \sqrt{\sum_{i=1}^{n}(H_{sat}^{(i)} - \bar{H}_{sat})^2/(n(n-1))}$ with $n = 5$ is 52 Oe. Earlier studies reported that the H_{sat} is close to H_c [33] or the value determined by the most stable state of a finite-sized system [37]. We thus assume that $\bar{H}_{sat} - \Delta H_{sat} \leqslant H_c \leqslant \bar{H}_{sat} + \Delta H_{sat}$. From these data, we

TABLE I. $H_{\rm jump}(\theta)$ and $H_{\rm sat}(\theta)$ at 10 K for the three samples A, B, and C. The magnetic fields are perpendicular to the helical axis and tilted from the plane of the platelet by the angle θ. The angle $\theta = 90^\circ(0^\circ)$ corresponds to the configuration of the least (most) demagnetization effect. The sample B and C were used, respectively, in Ref. [33] and its supplemental material.

	θ	$H_{\rm jump}$/Oe	$H_{\rm sat}$/Oe	$H_{\rm jump}/H_{\rm sat}$	$(H_{\rm sat} - H_{\rm jump})$/Oe
A	90°	775 ± 25	2025 ± 25	0.383	1250 ± 50
	90°	775 ± 25	1875 ± 25	0.413	1100 ± 50
	90°	775 ± 25	1725 ± 25	0.449	950 ± 50
	90°	775 ± 25	1975 ± 25	0.392	1200 ± 50
	90°	775 ± 25	1875 ± 25	0.413	1100 ± 50
B	90°	892.5 ± 2.5	2147.5 ± 2.5	0.416	1255 ± 5
	90°	892.5±2.5	2202.5±2.5	0.405	1310 ± 5
	90°	892.5±2.5	2187.5±2.5	0.408	1295 ± 5
	0°	1967.5±2.5	3082.5±2.5		1115 ± 5
C	90°	710 ± 10	1770 ± 10	0.404	1060 ± 20
	0°	1890 ± 10	2970 ± 10		1080 ± 20

obtain

$$0.385 \leqslant H_{\rm b}/H_{\rm c} \leqslant 0.434 \tag{13}$$

which agrees with the theoretical result Eq. (9) with the relative errors +7% and −5%. As more simple estimation, we just list the ratio of the median of $H_{\rm jumb}$ and that of $H_{\rm sat}$ in each run in Table I. We consider other samples. The sample B, which was used in Ref. [33], has the dimensions 10 μm square plane and 1 μm thickness (10 μm width along the c axis). $H_{\rm jump}$ and $H_{\rm sat}$ of the sample B are listed in Table I. We see that $H_{\rm jump}$ is highly reproducible while $H_{\rm sat}$ are scattered. We assume that $H_{\rm jump} \sim H_{\rm b}$ again and further assume that $H_{\rm sat} \sim H_{\rm c}$. For the configuration of the least demagnetization effect (see the data for B with $\theta = 90^\circ$ in Table I), we then obtain

$$H_{\rm b}/H_{\rm c} = 0.416, 0.405, 0.408, \tag{14}$$

which are close to the theoretical value Eq. (9). In the supplemental material of Ref. [33], they reported that $H_{\rm jump} =$ 720 Oe and $H_{\rm sat}$=1780 Oe for another sample (sample C) with dimension 13 μm square plane and 0.5 μm thickness (13 μm width along the c axis). We obtain

$$H_{\rm b}/H_{\rm c} = 0.404, \tag{15}$$

which is also close to Eq. (9).

Next we consider the demagnetization effect. In Ref. [33], the MR results for specimen C have been reported under the external magnetic field perpendicular to the c axis with various angles θ from the normal direction of the plane. We assume that magnetic field H inside specimen, external magnetic field $H_{\rm ex}$ and magnetization M are spatially uniform and parallel to one another in the FFM state for $\theta = 0^\circ$ and 90°. Then the relation $H = H_{\rm ext} - N_{\rm d}(\theta)M(H)$ with demagnetization factor $N_{\rm d}(\theta)$ holds for $H \geqslant H_{\rm b}$ in the decreasing field process. Experimentally observed fields $H_{\rm jump}$ and $H_{\rm sat}$ depend on θ and are related to $H_{\rm b}$ and $H_{\rm c}$ via

$$H_{\rm c} = H_{\rm sat}(\theta) - N_{\rm d}(\theta)M(H_{\rm c}) \tag{16}$$

$$H_{\rm b} = H_{\rm jump}(\theta) - N_{\rm d}(\theta)M(H_{\rm b} + 0). \tag{17}$$

Subtracting both hand sides of Eq. (17) from Eq. (16) and ignoring the difference $M(H_{\rm b} + 0)$ and $M(H_{\rm c})$, we obtain

$$H_{\rm sat}(\theta) - H_{\rm jump}(\theta) = H_{\rm c} - H_{\rm b} = (1 - 4/\pi^2)H_{\rm c}, \tag{18}$$

i.e., $H_{\rm sat}(\theta) - H_{\rm jump}(\theta)$ does not depend on whether $\theta = 0^\circ$ or 90° within this approximation. In Table I, we see that $H_{\rm sat}(\theta) - H_{\rm jump}(\theta)$ is independent of θ within relative error 10% in the specimen B and 5% in the specimen C.

V. DISCUSSION

The surface barrier was discussed theoretically first in the context of type II superconductors more than fifty years ago [4,5]. However, no sharp transitions related to vortex entrance into the samples have been observed experimentally. The reason was attributed to surface irregularities, which results in the inhomogeneities of fields near the surface [4,5]. Thus, the large jump of MR in the decreasing field process in chiral magnets is important as the first observation of large discontinuity due to the disappearance of the surface barrier of topological defects.

de Gennes [28] remarked that hysteresis is often observed in nucleation-type continuous phase transition between an ordered state that is an assembly of topological defects and the other phase without them. Examples of this type of transition include the lower critical field in type II superconductors, Dzyaloshinskii transition of the chiral soliton lattice [25] and cholesteric-nematic transition [22–24] in liquid crystals. Without strong perturbation to overcome topological metastability, the number of topological defects can change only by entrance or escape through the surface. Thus the surface barrier can be an intrinsic origin of hysteresis in nucleation-type continuous phase transitions in various systems. In conclusion, our study shows that the large jump of MR in $CrNb_3S_6$ is a clear phenomenon related to the surface barrier, which results from topological metastability.

Note added in proof. Recently, the CSL was confirmed in $YbNi_3Al_9$ through MR measurements [56]. This CSL has a short period (3.4 nm in zero field), in contrast to that in $CrNb_3S_6$, where the period in zero field is about 48 nm.

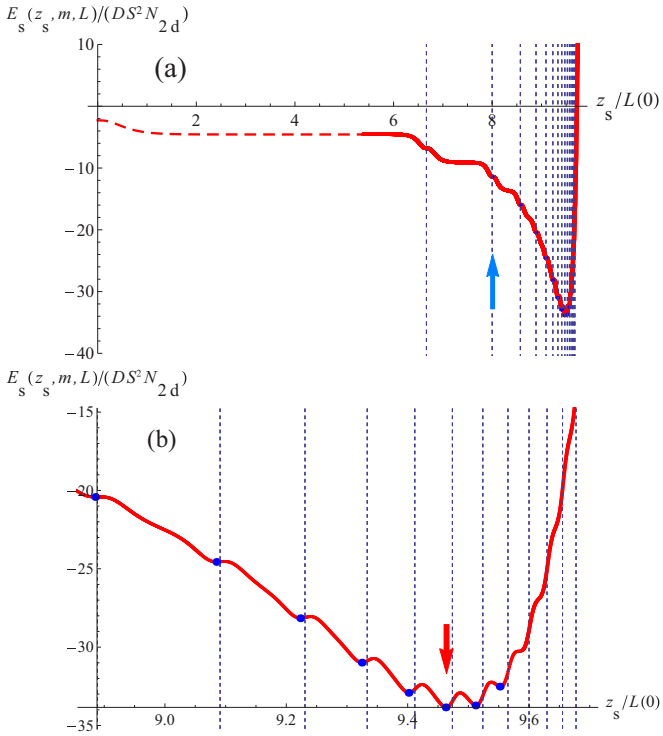

FIG. 5. Energy profile $E_s(z_s,m_b)$ as a function of z_s. (a) The red curve represents $E_s(z_s,m_b,20L(0))$ as a function of z_s. The red dotted curve represents twice the energy of single soliton $E_s(z_s,m_b)$ for a semi-infinite system. The vertical dashed lines represent $z_s = nL(0)/(2n+1)$, for which the intersoliton distance $(L-2z_s)$ becomes commensurate with the system size L. The local minima in the red curve are denoted by the blue dots. The arrow indicates the left-most local minimum, by the coordinate of which we defined $z_s(m)$. (b) Magnified view of the upper panel near the global minimum, which is indicated by the red arrow.

Understanding of properties of short-period CSL is an important future issue.

ACKNOWLEDGMENTS

The authors thank M. Mito, H. Ohsumi, J. Ohe, A. N. Bogdanov, and A. O. Leonov for their useful discussions. They also thank J. Kishine and K. Inoue for their continuous interest. M.S. and Y.K. acknowledge T. L. Monchesky for discussions on nucleation-type phase transition during the DMI conference in May 2017. Y.K. acknowledges K. Arimitsu for his comments on our manuscript. Preliminary computations in this work have been done using the facilities of the Supercomputer Center, the Institute for Solid State Physics, the University of Tokyo. This work was supported by Japan Society for the Promotion of Science (JSPS) KAKENHI Grants No. JP16J00091, No. JP17H02923, No. JP17H02767, and No. JP25220803. This work was also supported by Chirality Research Center (Crescent) in Hiroshima University, the Mext program for promoting the enhancement of research universities, Japan, JSPS and Russian Foundation for Basic Research (RFBR) under the Japan - Russia Research Cooperative Program, and JSPS Core-to-Core Program, A. Advanced Research Networks.

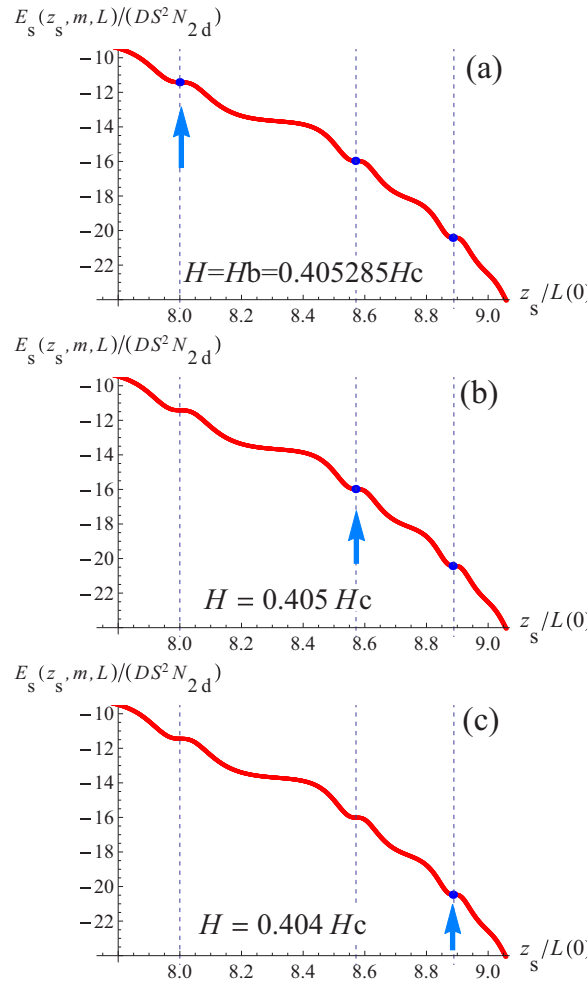

FIG. 6. Magnified view of $E_s(z_s,m)$ (red curve) as a function of z_s for (a) $H = H_b$, (b) $H = 0.405H_c$, and (c) $H = 0.404H_c$. The local minima are denoted by blue dots. The blue arrows indicate the leftmost local minima. The vertical dashed lines are the same as those in Fig. 5.

APPENDIX

The metastable state at m in the decreasing field process is specified by $z_s(m)$, which is defined by the local minimizer of $E_s(z_s,m,L)$ with the smallest z_s. Figure 5 shows $E_s(z_s,m_b,20L(0))$ as a function of z_s by the red curve (the lower panel is a magnified view of the upper panel). This red curve is practically independent of z_s for $z_s \leqslant 6L(0)$ and approaches the red dotted curve, which represents twice the energy of a single soliton for the semi-infinite system [Eq. (6)]. The local minima (blue dots) in the red curve are located near the crossing points with the vertical dashed lines. Those lines represent the commensurate condition for intersoliton distance with the system size.

With use of this diagram, we explain the evolution of the metastable state in the decreasing field process. At $H = H_b + 0$, the soliton is located at the surface $z_s(m_b + 0) = 0$. At $H = H_b - 0$, the state with $z_s = 0$ becomes unstable and the soliton state evolves to a local minimum [with $z_s(m_b - 0) \sim 8L(0)$] that is accessible with energy relaxing monotonically

from $z_s = 0$ to $z_s(m_b - 0)$. The existence of local minima and maxima is clearly shown in the lower panel of Fig. 5. We thus see that those structures in the energy landscape hinder the state to reach the global stable state, which is indicated by the red arrow in the lower panel. We see in the lower panel that the depth of the local minimum is shallower for smaller z_s when $z_s \leqslant 9.4L(0)$. We note a shoulder in the red curve near $z_s \sim 6.6L(0)$ in the upper panel of Fig. 5 and this is not a local minimum. The shallow local minima at $z_s/L(0) = 8, 8.56, 8.8$ causes an avalanchelike entrance of soliton slightly below $H = H_b$ in the decreasing field process. Figure 6 shows the blowup of $E_s(z_s, m)$ near $m = m_b$ ($H = H_b$). Slight decrease in m makes the leftmost local minimum unstable and induces successive entrance of solitons.

[1] P. W. Anderson, *Basic Notions of Condensed Matter Physics* (Addison-Wesley Publishing Company, New York, 1983).

[2] A. J. Leggett, *Quantum Liquids* (Oxford University Press, Oxford, 2006).

[3] A. A. Abrikosov, *Fundamentals of the Theory of Metals* (Elsevier Science Publishers, Amsterdam, 1988).

[4] C. P. Bean and J. D. Livingston, Phys. Rev. Lett. **12**, 14 (1964).

[5] P. G. de Gennes, *Superconductivity of Metals and Alloys* (Benjamin inc., New York, 1966), p. 76.

[6] E. Zeldov, A. I. Larkin, V. B. Geshkenbein, M. Konczykowski, D. Majer, B. Khaykovich, V. M. Vinokur, and H. Shtrikman, Phys. Rev. Lett. **73**, 1428 (1994).

[7] A. N. Bogdanov and D. A. Yablonskii, Zh. Eksp. Teor. Fiz. **95**, 178 (1989) [Sov. Phys. JETP **68**, 101 (1989)].

[8] A. Bogdanov and A. Hubert, J. Magn. Magn. Mater. **138**, 255 (1994); **195**, 182 (1999).

[9] S. Mühlbauer, B. Binz, F. Jonietz, C. Pfleiderer, A. Rosch, A. Neubauer, R. Georgii, P. Böni, Science **323**, 915 (2009).

[10] X. Z. Yu, Y. Onose, Y. Kanazawa, J. H. Park, J. H. Han, Y. Matsui, N. Nagaosa, and Y. Tokura, Nature (London) **465**, 901 (2010).

[11] N. Nagaosa and Y. Tokura, Nat. Nanotechnol. **8**, 899 (2013).

[12] A. Fert, V. Cros, and J. Sampaio, Nat. Nanotechnol. **8**, 152 (2013).

[13] J. Sampaio, V. Cros, S. Rohart, A. Thiaville, and A. Fert, Nat. Nanotechnol. **8**, 839 (2013).

[14] J. Iwasaki, M. Mochizuki, and N. Nagaosa, Nat. Nano **8**, 742 (2013).

[15] W. Koshibae and N. Nagaosa, Nat. Commun. **5**, 5148 (2014).

[16] W. Koshibae, Y. Kaneko, J. Iwasaki, M. Kawasaki, Y. Tokura, and N. Nagaosa, Jpn. J. Appl. Phys. **54**, 053001 (2015).

[17] M. Mochizuki and Y. Watanabe, Appl. Phys. Lett. **107**, 082409 (2015).

[18] J. Hagemeister, N. Romming, K. von Bergmann, E. Y. Vedmedenko, and R. Wiesendanger, Nat. Commun. **6**, 8455 (2015).

[19] H. Du, R. Che, L. Kong, X. Zhao, C. Jin, C. Wang, J. Yang, W. Ning, R. Li, C. Jin, X. Chen, J. Zang, Y. Zhang, and M. Tian, Nat. Commun. **6**, 8504 (2015).

[20] J. Müller, A. Rosch, and M. Garst, New J. Phys. **18**, 065006 (2016).

[21] P. G. de Gennes and J. Prost, *The Physics of Liquid Crystals*, 2nd ed. (Oxford Science Publications, Oxford, 1995).

[22] P. G. de Gennes, Solid State Commun. **6**, 163 (1968).

[23] G. Durand, L. Leger, F. Rondeles, and M. Veyssie, Phys. Rev. Lett. **22**, 227 (1969).

[24] R. B. Meyer, Appl. Phys. Lett. **14**, 208 (1969).

[25] I. E. Dzyaloshinskii, Zh. Eksp. Teor. Fiz. **47**, 992 (1964) [Sov. Phys. JETP **20**, 665 (1965)].

[26] Y. Togawa, T. Koyama, K. Takayanagi, S. Mori, Y. Kousaka, J. Akimitsu, S. Nishihara, K. Inoue, A. S. Ovchinnikov, and J. Kishine, Phys. Rev. Lett. **108**, 107202 (2012).

[27] Y. Togawa, Y. Kousaka, S. Nishihara, K. Inoue, J. Akimitsu, A. S. Ovchinnikov, and J. Kishine, Phys. Rev. Lett. **111**, 197204 (2013).

[28] P. de Gennes, in *Fluctuations, Instabilities and Phase Transitions*, edited by T. Riste, NATO ASI Series B Vol. 2 (Plenum, New York, 1975).

[29] T. Moriya and T. Miyadai, Solid State Commun. **42**, 209 (1982).

[30] T. Miyadai, K. Kikuchi, H. Kondo, S. Sakka, M. Arai, and Y. Ishikawa, J. Phys. Soc. Jpn. **52**, 1394 (1983).

[31] Y. Togawa, Y. Kousaka, K. Inoue, and J. Kishine, J. Phys. Soc. Jpn. **85**, 112001 (2016).

[32] Yu. A. Izyumov, Sov. Phys. Usp. **27**, 845 (1985).

[33] Y. Togawa, T. Koyama, Y. Nishimori, Y. Matsumoto, S. McVitie, D. Mc-Grouther, R. L. Stamps, Y. Kousaka, J. Akimitsu, S. Nishihara, K. Inoue, I. G. Bostrem, V. E. Sinitsyn, A. S. Ovchinnikov, and J. Kishine, Phys. Rev. B **92**, 220412 (2015).

[34] K. Tsuruta, M. Mito, Y. Kousaka, J. Akimitsu, J. Kishine, Y. Togawa, H. Ohsumi, and K. Inoue, J. Phys. Soc. Jpn. **85**, 013707 (2016).

[35] K. Tsuruta, M. Mito, Y. Kousaka, J. Akimitsu, J. Kishine, Y. Togawa, and K. Inoue, J. Appl. Phys. **120**, 143901 (2016).

[36] F. J. T. Goncalves, T. Sogo, Y. Shimamoto, Y. Kousaka, J. Akimitsu, S. Nishihara, K. Inoue, D. Yoshizawa, M. Hagiwara, M. Mito, R. L. Stamps, I. G. Bostrem, V. E. Sinitsyn, A. S. Ovchinnikov, J. Kishine, and Y. Togawa, Phys. Rev. B **95**, 104415 (2017).

[37] L. Wang, N. Chepiga, D.-K. Ki, L. Li, F. Li, W. Zhu, Y. Kato, O. S. Ovchinnikova, F. Mila, I. Martin, D. Mandrus, and A. F. Morpurgo, Phys. Rev. Lett. **118**, 257203 (2017).

[38] J. Yonemura, Y. Shimamoto, T. Kida, D. Yoshizawa, Y. Kousaka, S. Nishihara, F. J. T. Goncalves, J. Akimitsu, K. Inoue, M. Hagiwara, and Y. Togawa, Phys. Rev. B **96**, 184423 (2017).

[39] M. Mito, H. Ohsumi, K. Tsuruta, Y. Kotani, T. Nakamura, Y. Togawa, M. Shinozaki, Y. Kato, J-i. Kishine, J-i. Ohe, Y. Kousaka, J. Akimitsu, and K. Inoue, Phys. Rev. B **97**, 024408 (2018).

[40] Reproducible hysteresis in field-sweep and heat-sweep processes has been observed also in FeRh stripes by V. Uhlíř, J. A. Arregi, and E. E. Fullerton, Nat. Commun. **7**, 13113 (2016).

[41] J. Kishine and A. S. Ovchinnikov, Solid State Phys. **66**, 1 (2015).

[42] E. T. Whittaker and G. N. Watson, *A Course of Modern Analysis* (Cambridge University Press, New York, 1927).

[43] F. Garcia-Sanchez, P. Borys, A. Vansteenkiste, J.-V. Kim, and R. L. Stamps, Phys. Rev. B **89**, 224408 (2014).

[44] S. A. Meynell, M. N. Wilson, H. Fritzsche, A. N. Bogdanov, and T. L. Monchesky, Phys. Rev. B **90**, 014406 (2014).
[45] M. N. Wilson, E. A. Karhu, D. P. Lake, A. S. Quigley, S. Meynell, A. N. Bogdanov, H. Fritzsche, U. K. Rößler, and T. L. Monchesky, Phys. Rev. B **88**, 214420 (2013).
[46] H. F. Du, W. Ning, M. L. Tian, and Y. H. Zhang, Europhys. Lett. **101**, 37001 (2013).
[47] H. F. Du, W. Ning, M. L. Tian, and Y. H. Zhang, Phys. Rev. B **87**, 014401 (2013).
[48] S. Rohart and A. Thiaville, Phys. Rev. B **88**, 184422 (2013).
[49] F. N. Rybakov, A. B. Borisov, and A. N. Bogdanov, Phys. Rev. B **87**, 094424 (2013).
[50] F. N. Rybakov, A. B. Borisov, S. Blügel, and N. S. Kiselev, New J. Phys. **18**, 045002 (2016).
[51] K. M. D. Hals and K. Everschor-Sitte, Phys. Rev. Lett. **119**, 127203 (2017).
[52] The soliton coordinate z_s reduces to that denoted by the same symbol for a semi-infinite system [see Eq. (5)] when the state with at most two solitons inside the magnets with dimension $L \gg L(0)$.
[53] The magnetization curve of the ground state in finite-sized system under the *fixed* boundary condition has been calculated in Ref. [54] while the red dotted line in Fig. 4 represents that under the *free* boundary condition.
[54] J.-i. Kishine, I. G. Bostrem, A. S. Ovchinnikov, and V. E. Sinitsyn, Phys. Rev. B **89**, 014419 (2014).
[55] Strictly speaking, the critical field $H_c(L)$ in finite-sized systems depend on the system size but deviation from that in the thermodynamic limit is negligibly small for the system with $L = 20L(0)$ shown in Fig. 4 .
[56] R. Aoki, Y. Togawa, and S. Ohara, Phys. Rev. B **97**, 214414 (2018).